CONF-950740--81

RESPONSE OF WAVE EXCITED OFFSHORE PLATFORMS

Shih-Jung Chang

Research Reactors Division
Oak Ridge National Laboratory
Oak Ridge, Tennessee

Guillermo D. Hahn

Department of Civil and Environmental Engineering
Vanderbilt University
Nashville, Tennessee

Outline of paper to be presented at
ASME/JSME Pressure Vessel and Piping Conference
Honolulu, Hawaii
July 24-27, 1995

Prepared by the
Research Reactors Division
OAK RIDGE NATIONAL LABORATORY
Oak Ridge, Tennessee 37831
managed by
MARTIN MARIETTA ENERGY SYSTEMS, INC.
for the
U.S. DEPARTMENT OF ENERGY
under contract DE-AC05-84OR21400

DISCLAIMER

Portions of this document may be illegible in electronic image products. Images are produced from the best available original document.

RESPONSE OF WAVE EXCITED OFFSHORE PLATFORMS

Guillermo D. Hahn
Department of Civil and Environmental Engineering
Vanderbilt University
Nashville, Tennessee

Shih-Jung Chang
Research Reactors Division
Oak Ridge National Laboratory
Oak Ridge, Tennessee

ABSTRACT

A study of the resultants of the inertia and drag force components induced by waves on offshore structures is made, and the relationships between these resultants and the corresponding modal forces that govern the structural response are examined. The information and concepts reported elucidate the main factors that control such forces. Using the deep-water approximation of linear wave theory and the Morison equation, it is shown that the inertia and drag components of the modal forces can be expressed in terms of the sea surface kinematics. This treatment of the wave excitations advances the understanding of their characteristics and contributes to forming a basis for efficient, reliable evaluations of the response of wave-excited offshore platforms.

INTRODUCTION

Evaluations of the dynamic response of wave-excited offshore structures are usually made by calculating the wave force intensities by applications of the Morison equation (Morison et al. 1950, Sarpkaya and Isaacson 1981). Such applications lead to the definition of the wave excitation in terms of its inertia and drag force-intensity components. In the application of the modal superposition method (Clough and Penzien 1993), spatial integrals of products of these force intensities and the modal shapes of the structure are calculated to obtain the generalized or modal forces that control the response. The demonstration that the modal forces can be expressed in terms of the sea surface kinematics is a distinguishing feature of the present study. Examinations are first made of the magnitudes of the resultants of the inertia and drag force intensities and of the positions of their lines of action; and this is followed by analyses that establish the relationships between the resultants and the corresponding modal forces, leading to the identification of the main factors that govern these forces and to useful related concepts. Analyses for the resulting structural response are also made, further enhancing the value of the reported investigation. The modal responses examined are computed for wide ranges of values of natural frequencies. The study applies to steel, jacket-type platforms operating in relatively deep waters, for which the deep-water approximation of linear wave theory is appropriate.

INERTIA FORCE RESULTANT

In order to calculate the inertia force resultant, the structure is modeled as a cantilever system. Let $q_m(y,t)$ be the inertia force intensity (force per unit of length along the height of the structure) acting on the

structure at a distance y from the still water level (SWL), at time t; and let D be the total water depth. The resultant of these force intensities, $R_m(t)$, and the position of the line of action of this resultant from the SWL, $y_m(t)$, are defined by

$$R_m(t) = \int_0^D q_m(y,t)\,dy \tag{1}$$

$$y_m(t) = \frac{1}{R_m(t)} \int_0^D y\, q_m(y,t)\,dy \tag{2}$$

in which

$$q_m(y,t) = B_m(y)\ \ddot{u}(y,t) \tag{3}$$

where $\ddot{u}(y,t)$ = horizontal water particle acceleration; $B_m(y) = c_m(y)\ \rho\ V(y)$; $c_m(y)$ = inertia force coefficient; ρ = mass density of the fluid; and $V(y)$ = structural volume per unit of length.

Using the deep-water approximation of linear wave theory (Sarpkaya and Isaacson 1981), the water particle acceleration may be expressed as

$$\ddot{u}(y,t) = -\sum_{i=1}^{n} \exp(-\omega_i^2 \frac{y}{g})\,\omega_i^2\ a_i \sin(\omega_i\ t - \theta_i) \tag{4}$$

where g = gravitational acceleration; ω_i = frequency in rad/sec; a_i = displacement amplitude corresponding to ω_i; and the θ_i's are random phase angles uniformly distributed between 0 and 2π. The quantities ω_i and a_i may be obtained by sampling an applicable wave spectrum, such as the Pierson-Moskowitz wave spectrum (Pierson and Moskowitz 1964), at n points.

An important concept can be developed by assuming that $B_m(y) = B_m$ = constant. This assumption is not unrealistic because the cross sections of many designs of offshore platforms do not significantly vary with depth (des Deserts 1992). Under more general conditions to be examined later, however, the effects of the spatial variation of B_m are accounted for. Taking B_m as constant and assuming that D is large [i.e., $D >$ $\approx$ 300 m (1000 ft)], it can be shown that $R_m(t)$ in (1) is given by

$$R_m(t) = -B_m\, g\, u(0,t) \tag{5}$$

in which

$$u(0,t) = \sum_{i=1}^{n} a_i \sin(\omega_i\ t - \theta_i) \tag{6}$$

is the horizontal water particle displacement computed at the SWL.

The resultant of the inertia forces, under the conditions examined, does not ultimately depend on the characteristics of the water particle accelerations, as (1) and (3) suggest. It is governed by $u(0,t)$, as demonstrated by (5); and this finding represents the first of the important concepts introduced herein.

Furthermore, provided that B_m is constant and the structure operates in relatively deep waters, it can be shown that the position of the line of action of the inertia force resultant is given by

$$y_m(t) = -g\ \frac{u^{xx}(0,t)}{u(0,t)} \tag{7}$$

where

$$u^{xx}(0,t) = -\sum_{i=1}^{n} \frac{1}{\omega_i^2} a_i \sin(\omega_i\ t - \theta_i) \tag{8}$$

is the second integral of $u(0,t)$ with respect to time. Another important concept is identified by (7): the position of the line of action of the resultant of the inertia force intensities is proportional to the ratio of the second time integral of $u(0,t)$ to $u(0,t)$.

DRAG FORCE RESULTANT

The resultant of the drag force intensities can be expressed in terms of the horizontal fluid particle velocity, $\dot{u}(y,t)$, as

$$R_d(t) = \int_0^D B_d(y)\,|\dot{u}(y,t)|\dot{u}(y,t)\,dy \tag{9}$$

in which $B_d(y) = 0.5 c_d(y)\,\rho\,A(y)$; $c_d(y)$ = the drag force coefficient; and $A(y)$ = the projected area of the structure per unit of length. An improved definition for $R_d(t)$ can be obtained by replacing $\dot{u}(y,t)$ in (9) with the relative fluid-structure velocity to account for the effects of the so-called fluid-structure interaction. Although these effects have been the subject of previous studies (e.g., Veletsos et al. 1988) and are known to effectively increase the damping of the system, there remains a need for methods that can predict the increases in damping for realistic multi-degree of freedom systems. However, the evaluation of such increases is beyond the scope of the present study and will be the subject of future examinations.

It is convenient in this analysis to work with the absolute value of $R_d(t)$, approximately taken as

$$|R_d(t)| \approx \int_0^D B_d(y)\,\dot{u}^2(y,t)\,dy \tag{10}$$

in which

$$\dot{u}^2(y,t) = \left[\sum_{i=1}^{n} \exp(-\omega_i^2 \frac{y}{g})\,\omega_i\,a_i \cos(\omega_i t - \theta_i)\right] \times \left[\sum_{j=1}^{n} \exp(-\omega_j^2 \frac{y}{g})\,\omega_j\,a_j \cos(\omega_j t - \theta_j)\right] \tag{11}$$

The approximation of (10) is based on the assumption that the sign of $\dot{u}(y,t)$ is independent of y. This assumption is acceptable. Substituting (11) into (10), taking B_d = constant, and evaluating the integral in (10) by assuming that D is large lead to

$$|R_d(t)| \approx B_d\,g \sum_{i=1}^{n}\sum_{j=1}^{n} F(\xi)\,a_i\,a_j \cos(\omega_i t - \theta_i) \times \cos(\omega_j t - \theta_j) \tag{12}$$

where $F(\xi) = \xi/(1+\xi^2)$; and $\xi = \omega_j/\omega_i$. The dimensionless function $F(\xi)$ is smooth and attains a peak value of 0.5 at $\xi = 1$. Because displacement wave spectra tend to cover a narrow band of frequencies, the products $(a_i\,a_j)$ in (12) are relatively small for $\xi < \approx 0.5$ and $\xi > \approx 2$. It is therefore proposed that the function $F(\xi)$ be replaced with its average computed over the range $0.5 < \xi < 2$. This average is 0.46, and $R_d(t)$ is then approximately given by

$$R_d(t) \approx 0.46\,B_d\,g\,|v(0,t)|v(0,t) \tag{13}$$

where

$$v(0,t) = \eta(t) = \sum_{i=1}^{n} a_i \cos(\omega_i t - \theta_i) \tag{14}$$

is the vertical water particle displacement corresponding to the SWL.

The resultant of the drag force intensities is not governed, under the conditions examined, by the square of the fluid particle velocities, as (9) appears to suggest. It is ultimately controlled by the square of the vertical displacement computed at the SWL, as indicated by (13). This is another important concept. It will be shown later that (13) indeed provides an excellent approximation for $R_d(t)$.

The position of the line of action of the resultant of the drag forces from the SWL is defined by

$$y_d(t) = \frac{1}{R_d(t)} \int_0^D y\,B_d(y)\,|\dot{u}(y,t)|\dot{u}(y,t)\,dy \tag{15}$$

and its absolute value is approximately taken as

$$|y_d(t)| \approx \frac{1}{|R_d(t)|} \int_0^D y\,B_d(y)\,\dot{u}^2(y,t)\,dy \tag{16}$$

Assuming that B_d is constant and D is large, integration of (16) leads to

$$|y_d(t)| \approx \frac{1}{|R_d(t)|} B_d\,g^2 \sum_{i=1}^{n}\sum_{j=1}^{n} F^2(\xi) \times \frac{a_i\,a_j}{\omega_i\,\omega_j} \cos(\omega_i t - \theta_i)\cos(\omega_j t - \theta_j) \tag{17}$$

The average of $F^2(\xi)$ over the range $0.5 < \xi < 2$ is about $(0.46)^2$, and replacing $F^2(\xi)$ in (17) with this average leads to

$$y_d(t) \approx -0.46\, g\, \frac{|u^x(0,t)|\, u^x(0,t)}{|v(0,t)|\, v(0,t)} \tag{18}$$

in which

$$u^x(0,t) = -\sum_{i=1}^{n} \frac{1}{\omega_i}\, a_i \cos(\omega_i t - \theta_i) \tag{19}$$

is the first integral of $u(0,t)$ with respect to time. It is observed in (18) that $y_d(t)$ depends on $u^x(0,t)$ and $v(0,t)$, which are histories associated with the sea surface kinematics. This represents an additional important concept.

RELATIONSHIPS BETWEEN RESULTANTS AND MODAL FORCES

This section establishes the relationships between the resultants previously defined and modal forces calculated for a particular, linearly varying modal shape. A limited assessment of modal forces corresponding to other modal shapes is made later.

Consider the first modal response of an offshore structure which is induced by the first modal inertia and drag forces. Assume that the first modal shape, $\phi(y)$, varies linearly from zero at the sea floor level, and that it is normalized so that its ordinate corresponding to the SWL is unity. Under these conditions, the first modal inertia and drag forces, $P_m^*(t)$ and $P_d^*(t)$, respectively, defined by

$$P_m^*(t) = \int_0^D \phi(y)\, B_m\, \tilde{u}(y,t)\, dy \tag{20a}$$

$$P_d^*(t) = \int_0^D \phi(y)\, B_d\, |\dot{u}(y,t)|\dot{u}(y,t)\, dy \tag{20b}$$

reduce to

$$P_m^*(t) = R_m(t)\left[1 - \frac{y_m(t)}{D}\right] \tag{21a}$$

$$P_d^*(t) = R_d(t)\left[1 - \frac{y_d(t)}{D}\right] \tag{21b}$$

in which B_m and B_d are assumed to be constants. It is apparent in (21a-b) that the modal forces depend on the resultants $R_m(t)$ and $R_d(t)$, and on the positions of these resultants, $y_m(t)$ and $y_d(t)$. For very deep waters, however, it can be shown that the ratios $y_m(t)/D$ and $y_d(t)/D$ are small, and the modal forces only depend on the resultants in this case.

It is of interest to further examine these first modal inertia and drag forces, and the corresponding structural responses. It is of particular interest to assess the accuracy of the approximate solution previously reported for the drag force component [i.e., (13) and (18)]. These examinations and assessments are made herein by considering a particular sea state numerically generated by using the deep-water approximation of linear wave theory and a Pierson-Moskowitz wave spectrum with a significant wave height of 12.2 m (40 ft) and a mean wave period of 12.5 s. The wave spectrum was sampled with a frequency increment of 0.005 Hz, and a high-frequency cut-off of 0.3 Hz was imposed. For this sea state, Fig. 1 presents the histories of $v(0,t)$, $u(0,t)$, $u^x(0,t)$ and $u^{xx}(0,t)$ and their respective absolute maximum values, v_o, u_o, u_o^x, and u_o^{xx}, denoted by Max in the figure. These are the histories associated with the sea surface kinematics which govern the definition of the modal forces given by (21a-b). For the generation implemented herein, the histories of water particle kinematics are periodic with a period of 200 sec.

First Modal Inertia Force and Associated Response

To obtain insight into the first modal inertia force, Fig. 2 presents histories of $R_m(t)$ and $y_m(t)$, and of $P_m^*(t)$ computed for D = 305 m, 610 m, and 915 m (1000, 2000, and 3000 ft). The forces shown in this figure are normalized with respect to $(R_m)_0$, the peak value of $R_m(t)$.

It is seen in Fig. 2 that the time variation of the resultant of the inertia force intensities, $R_m(t)$, is the same (with opposite sign) as that for $u(0,t)$ reported in Fig. 1 [this is a consequence of (5)]. It is also observed in Fig. 2 that the position of the resultant, $y_m(t)$, changes quite irregularly. However, when the magnitude of $R_m(t)$ is not small, $y_m(t)$ usually falls in the range 30-90 m (100-300 ft). In particular, when

the peak value of $R_m(t)$ is attained at time $t = t_m \approx 110$ s, $y_m(t_m) \approx 46$ m (150 ft – see Fig. 2); and this observation will help to explain some of the characteristics of the modal forces which are examined next.

The time variations of the modal forces reported in Fig. 2 are essentially the same as that of the resultant $R_m(t)$ itself. This is due to the fact that in deep waters, the term $[y_m(t)/D]$ in (21a) is much smaller than unity when the magnitude of $R_m(t)$ is not small, and, consequently, that term does not significantly influence such time variations. However, the peak values of the modal forces are seen in Fig. 2 to change with D in proportion with the factor $[1-y_m(t_m)/D]$, which is consistent with (21a).

Since changes in D primarily affect the peak value of the modal force, they will mainly influence the static response of the system, defined as the response induced by the static application of the peak value of the excitation. The effects of such changes on the dynamic response are small, as shown in Fig. 3. This figure reports response spectra for the maximum steady-state displacements of linear oscillators with natural frequencies, f, ranging from 0.01 to 1 Hz and 5% of critical damping. The steady-state response was obtained by repetitive applications of the excitation until the response became independent of the initial conditions. The amplification factor reported in the figure is defined as the ratio of the absolute maximum dynamic displacement of the oscillator to the corresponding static displacement induced by the peak value of the excitation. These spectra have been computed by using the modified Euler method (Hahn 1991) for the different modal forces shown in Fig. 2, and for $R_m(t)$ (i.e., the modal force for $D = \infty$); and it is observed that they are almost indistinguishable from each other, indicating, as expected, that changes in D do not particularly influence the dynamic response. It follows that for this particular modal force, the dynamic effects, expressed in terms of the amplification factor, may be approximately defined for practical purposes by only accounting for the characteristics of $R_m(t)$, which depends on $u(0,t)$.

First Modal Drag Force and Associated Response

Let $R_{dA}(t)$ be the approximation for $R_d(t)$ given by (13), and let $y_{dA}(t)$ be the approximation for $y_d(t)$ defined by (18). Also, let $P^*_{dA}(t)$ be the associated approximate modal force obtained from (21b), using $R_d(t) = R_{dA}(t)$ and $y_d(t) = y_{dA}(t)$. In addition, let $R_{dE}(t)$, $y_{dE}(t)$, and $P^*_{dE}(t)$ be the corresponding histories computed by means of highly accurate numerical evaluations of the integrals indicated in (9) (assuming B_d = constant), (15) and 20b. Because these integrals were calculated with a high degree of accuracy, the histories $R_{dE}(t)$, $y_{dE}(t)$, and $P^*_{dE}(t)$ may be assumed to be "exact."

Figure 4a shows plots of $R_{dA}(t)$, $y_{dA}(t)$, and $P^*_{dA}(t)$ computed for D = 305 m (1000 ft); and Fig. 4b presents the corresponding plots for $R_{dE}(t)$, $y_{dE}(t)$, and $P^*_{dE}(t)$. The forces reported in Fig. 4 are normalized with respect to $(R_{dA})_0$, the absolute maximum value of $R_{dA}(t)$; and the peak values of the normalized forces are identified in the figure. A comparison of the histories shown in Fig. 4a with those presented in Fig. 4b indicates that the approximations of (13) and (18) are indeed excellent. Note that the approximation overestimates the peak value of $R_d(t)$ and $P^*_d(t)$ by only 2% for the sea state considered, and the histories for $y_{dA}(t)$ and $y_{dE}(t)$ are quite similar, particularly when the magnitude of $R_d(t)$ is not small.

In Fig. 5 are presented response spectra computed for the modal forces, $P^*_{dA}(t)$ and $P^*_{dE}(t)$, shown in Fig. 4, and it is observed that they are almost indistinguishable from each other, further indicating that the approximate solution is quite accurate. A similar behavior is observed in Fig. 6, which shows response spectra computed for $R_{dA}(t)$ and $R_{dE}(t)$ (i.e., the approximate and "exact" modal forces for $D = \infty$).

Since the time variations of $P^*_{dA}(t)$ and $R_{dA}(t)$ are essentially the same (see Fig. 4), changes in D (for deep waters) do not influence the associated dynamic response, expressed in terms of the dynamic amplification factor. The position of the line of action of the resultant of the drag force, $y_d(t)$, is about half of that of the resultant of the inertia force, $y_m(t)$ (for a harmonic wave, $y_d = 0.5\, y_m$). Consequently, the effects of changes in the term involving D in (21b) are less significant than those of changes in the corresponding term in (21a). It is also of interest to point out that when $(R_{dA})_0$ is attained at time $t = t_d \approx 108$ (see Fig. 4a), $y_{dA}(t_d) \approx 24.4$ m (80 ft), and the peak value of $P^*_{dA}(t)$ reported in Fig. 4a is

essentially given by $[1-y_{dA}(t_d)/D](R_{dA})_o = 0.92(R_{dA})_0$, which is consistent with (21b).

The inertia and drag force components act simultaneously on the structure, and the data reported indicate that for B_m = constant, B_d = constant, and $\phi(y) = (1-y/D)$, the modal dynamic response induced by the combination of the inertia and drag forces is controlled by the histories of $u(0,t)$ and $|v(0,t)|\, v(0,t)$. It is also important to note that $R_m(t)$ and $R_d(t)$, defined by (5) and (13), are the base shear forces induced by the static application of the inertia and the drag forces (i.e., base shear forces computed by ignoring the inertia effects resulting from the acceleration of the mass of the structure and the hydrodynamic added mass); and the quantities $P_m^*(t)$ and $P_d^*(t)$, given by (21a-b), are the associated static base overturning moments divided by D. As demonstrated, these shear forces and overturning moments are governed by the sea surface kinematics.

ADDITIONAL CONSIDERATIONS

In the definition of the modal forces considered so far, it has been assumed that B_m and B_d are constants; and that the modal shape itself, $\phi(y)$, varies linearly. It is therefore of interest to examine the modal forces for other realistic distributions of $B_m(y)$, $B_d(y)$, and $\phi(y)$.

The inertia and drag modal forces may be generally expressed as

$$P_m^*(t) = \int_0^D B_m^*(y)\, \ddot{u}(y,t)\, dy \tag{22}$$

$$P_d^*(t) = \int_0^D B_d^*(y)\, |\dot{u}(y,t)|\dot{u}(y,t)\, dy \tag{23}$$

where $B_m^*(y) = \phi(y)\, B_m(y)$ and $B_d^*(y) = \phi(y)\, B_d(y)$. It is important to realize, however, that the wave action is significant only over a depth, D_e, of about 150 m (500 ft). Consequently, the integrals in (22) and (23) need to be evaluated only for $0 \le y \le D_e$. For deep waters where $D > D_e$, excellent approximations (for many practical cases) for $B_m^*(y)$ and $B_d^*(y)$ may be obtained over the range $0 \le y \le D_e$ by assuming that they vary linearly within this range. Appropriate linear approximations for $B_m^*(y)$ and $B_d^*(y)$ are:

$$\hat{B}_m^*(y) = B_{m0}^*\, (1+\beta_m \frac{y}{D}) \tag{24}$$

$$\hat{B}_d^*(y) = B_{d0}^*\, (1+\beta_d \frac{y}{D}) \tag{25}$$

in which $B_{m0}^* = B_m^*(0)$, $B_{d0}^* = B_d^*(0)$, and

$$\beta_m = -\frac{3}{2}\frac{D}{D_e} + \frac{3D}{D_e^3}\int_0^{D_e} y\, \frac{B_m^*(y)}{B_{m0}^*}\, dy \tag{26}$$

$$\beta_d = -\frac{3}{2}\frac{D}{D_e} + \frac{3D}{D_e^3}\int_0^{D_e} y\, \frac{B_d^*(y)}{B_{d0}^*}\, dy \tag{27}$$

These values of β_m and β_d minimize the integral over $0 \le y \le D_e$ of the square of the error between the linear approximations, $\hat{B}_m^*(y)$ and $\hat{B}_d^*(y)$, and the corresponding actual functions, $B_m^*(y)$ and $B_d^*(y)$.

Assuming that $B_m^*(y)$ and $B_d^*(y)$ can be approximated by $\hat{B}_m^*(y)$ and $\hat{B}_d^*(y)$, respectively, the modal forces may be expressed as

$$P_m^*(t) \approx R_m^*(t)\left[1+\beta_m \frac{y_m(t)}{D}\right] \tag{28a}$$

$$P_d^*(t) \approx R_d^*(t)\left[1+\beta_d \frac{y_d(t)}{D}\right] \tag{28b}$$

where

$$R_m^*(t) = -B_{m0}^*\, g\, u(0,t) \tag{29a}$$

$$R_d^*(t) = 0.46\, B_{d0}^*\, g\, |v(0,t)|v(0,t) \tag{29b}$$

and $y_m(t)$ and $y_d(t)$ are given by (7) and (18). For $\phi(y) = (1-y/D)$ and constants $B_m(y) = B_m$ and $B_d(y) = B_d$, $R_m^*(t) = R_m(t)$, $R_d^*(t) = R_d(t)$, $\beta_m = \beta_d = -1$, and (28a-b) reduce to (21a-b).

It is of interest to examine the appropriateness of the proposed linear approximations for systems characterized by functions $B_m^*(y)$ and $B_d^*(y)$ that do not vary linearly. To simplify the definition of these functions, the following two cases are considered as possible and representative:

Case 1: Uniform Cantilever Flexural Beam – First Mode. For this case, $B_m^*(y) = B_{m0}^*\ \phi(y)$, $B_d^*(y) = B_{d0}^*\ \phi(y)$, and (Young and Felgar 1949)

$$\phi(y) = \frac{1}{2}\left[\cosh\xi - \cos\xi - 0.7341(\sinh\xi - \sin\xi)\right] \quad (30)$$

where $\xi = 1.8751(1 - y/D)$.

Case 2: Uniform Cantilever Flexural Beam – Second Mode. In this case, $B_m^*(y) = B_{m0}^*\ \phi(y)$, $B_d^*(y) = B_{d0}^*\ \phi(y)$, and (Young and Felgar 1949)

$$\phi(y) = -\frac{1}{2}\left[\cosh\xi - \cos\xi - 1.0185(\sinh\xi - \sin\xi)\right] \quad (31)$$

where $\xi = 4.6941(1 - y/D)$.

Although these two cases have been defined for uniform systems [i.e., systems with constant $B_m(y)$ and $B_d(y)$], they also apply to nonuniform structures provided that the variations for $\hat{B}_m^*(y)$ and $\hat{B}_d^*(y)$ of these structures are similar to those considered herein. Figure 7 compares the linear approximations, $\hat{B}_m^*(y)$ and $\hat{B}_d^*(y)$, for Cases 1 and 2 with the corresponding exact functions, $B_m^*(y)$ and $B_d^*(y)$, for D = 305 m (1000 ft); and Fig. 8 shows a similar comparison for D = 915 m (3000 ft). It is seen in these figures that the linear variations approximate $B_m^*(y)$ and $B_d^*(y)$ very well over the region of interest (i.e., $0 \le y \le D_e$), particularly for the deep-water case of D = 915 m (3000 ft). The data of Figs. 7 and 8 have been normalized to obtain unity values at the SWL.

It should be noted that for the data of Fig. 7, $\beta_m = \beta_d = -1.348$ for Case 1, and $\beta_m = \beta_d = -4.024$ for Case 2. For the data of Fig. 8, $\beta_m = \beta_d = -1.374$ for Case 1, and $\beta_m = \beta_d = -4.735$ for Case 2. It should be further noted that changes in the variations of $B_m^*(y)$ and $B_d^*(y)$ lead to changes in β_m and β_d that, in turn, effectively lead to changes in the water depth, as can be appreciated in (28a-b). Note that these equations can be rewritten as

$$P_m^*(t) \approx R_m^*(t)\left[1 + \frac{y_m(t)}{D_m}\right] \quad (32a)$$

$$P_d^*(t) \approx R_d^*(t)\left[1 + \frac{y_d(t)}{D_d}\right] \quad (32b)$$

where $D_m = D/\beta_m$ and $D_d = D/\beta_d$ may be interpreted as effective water depths. It has been previously shown that, for deep waters, the main effect of changes in the water depth is to affect the peak value of the excitation and the associated static response of the system. Consequently, the corresponding dynamic effect, expressed in terms of the dynamic amplification factor, is primarily governed by the resultants, $R_m^*(t)$ and $R_d^*(t)$, even if the variations for $B_m^*(y)$ and $B_d^*(y)$ are not linear. The resultants, $R_m^*(t)$ and $R_d^*(t)$, given by (29a-b), depend on $u(0,t)$ and $v(0,t)$, the horizontal and vertical water particle displacements at the SWL.

CONCLUSION

Important characteristics of the wave forces that act on offshore platforms were identified. For a uniform structure (i.e., B_m and B_d are constants), the inertia and drag wave force resultants have been shown to be controlled by the horizontal and vertical fluid particle displacements, respectively, computed at the SWL. It has been further demonstrated that for a uniform structure with a linear modal shape, $\phi(y) = (1 - y/D)$, the inertia and drag modal forces can be expressed in terms of those resultants. Examinations were also made of nonuniform systems, and linear approximations were proposed that effectively reduce them to uniform systems with linearly varying modal shapes. The information and concepts reported in this study are useful, and further examinations are indeed needed to fully demonstrate their potential for contributing to improved designs of offshore structures. The pursuit of these examinations is beyond the scope of the present study. They will be made, however, in future presentations.

REFERENCES

Clough, R. H., and Penzien, J. (1993). Dynamics of structures, McGraw-Hill, New York, N.Y.

des Deserts, L. (1992). "Architecture and application of various configurations of compliant towers," *Proceedings of the 11th International Conference on Offshore Mechanics and Arctic Engineering*, Vol. I-B, ASME, New York, 471-484.

Gudmestad, O. T. (1993). "New concepts, environment and model testing," *Journal of Offshore Mechanics and Arctic Engineering*, ASME, Vol. 115, February, 5-6.

Hahn, G. D. (1991). "A modified Euler method for dynamic analyses." *Journal for Numerical Methods in Engineering*, Vol. 32, No. 5, 943-955.

Morison, J. R., O'Brien, M. P., Johnson, J. W., and Schaaf, S. A. (1950). "The force exerted by surface waves on piles." *Petroleum Transactions*, AIME, Vol. 189, 149-154.

Pierson, W. J., and Moskowitz, L. (1964). "A proposed spectral form for fully developed wind seas based on the similarity theory of S. A. Kitaigorodskii." *Journal of Geophysics Research*, Vol. 69, No. 24, 5181-5190.

Sarpkaya, T., and Isaacson, M. (1981). Mechanics of wave forces on offshore structures, Van Nostran Reinhold, New York, N.Y.

Veletsos, A. S., Prasad, A. M., and Hahn, G. D. (1988). "Fluid-structure interaction effects for offshore structures," *Journal of Earthquake Engineering and Structural Dynamics*, Vol. 16, 631-652.

Young, D., and Felgar, R. P. (1949). Tables of characteristic functions representing normal modes of vibration of a beam, The University of Texas Publication No. 4913, 19-21.

[1]Based on work performed at Oak Ridge National Laboratory, managed by Martin Marietta Energy Systems, Inc., for the U.S. Department of Energy under contract DE-AC05-84OR21400. Accordingly, the U.S. government retains a nonexclusive, royal-free license to publish or reproduce the published form of this contribution, or allow others to do so, for U.S. government purposes.

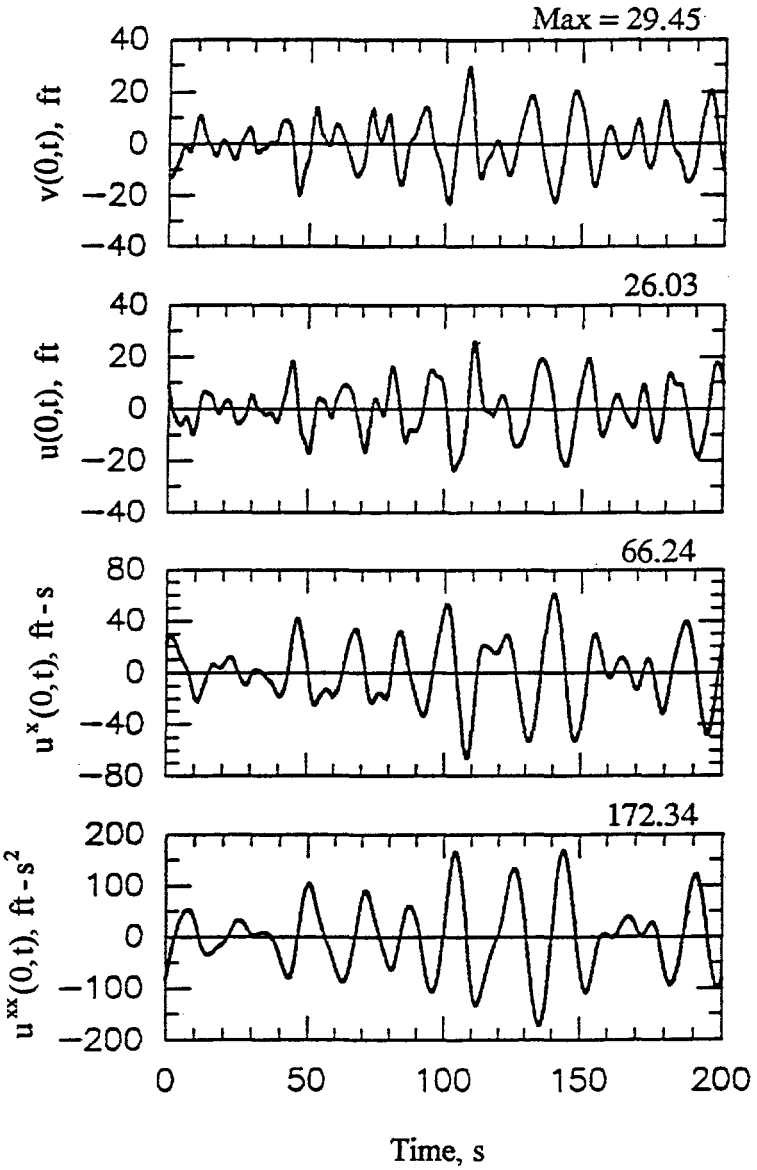

Fig. 1. Fluid-Particle Kinematics at the SWL for Sea State Considered.

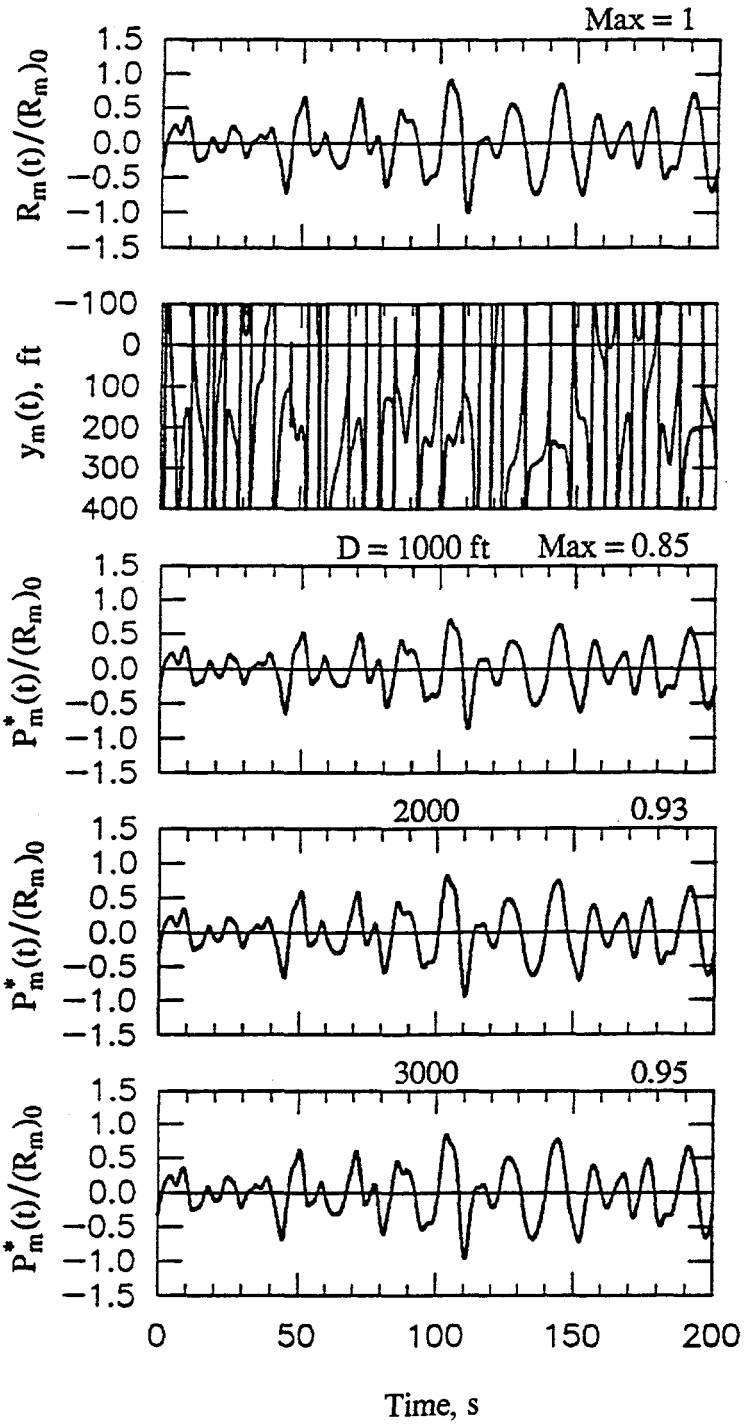

Fig. 2. Histories of $R_m(t)$, $y_m(t)$, and Corresponding Modal Forces.

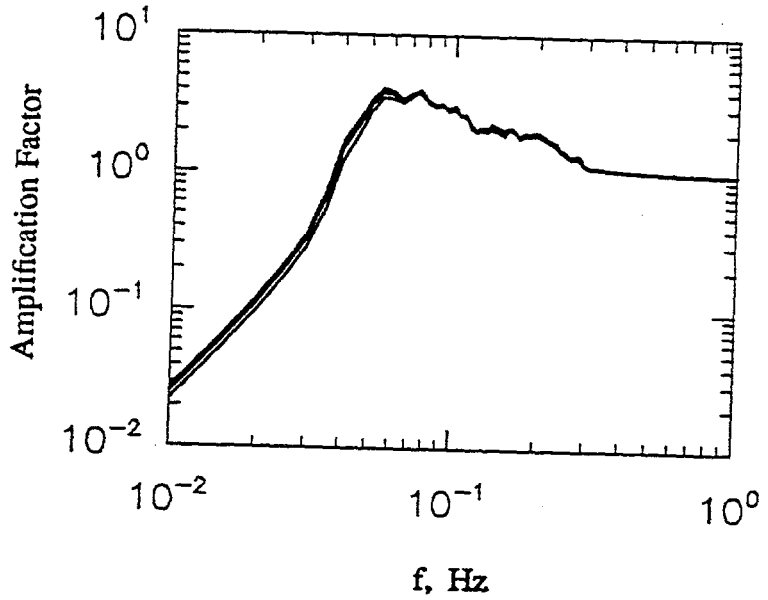

Fig. 3. Response Spectra for Inertia Forces Shown in Fig. 2; 5% Damping.

DISCLAIMER

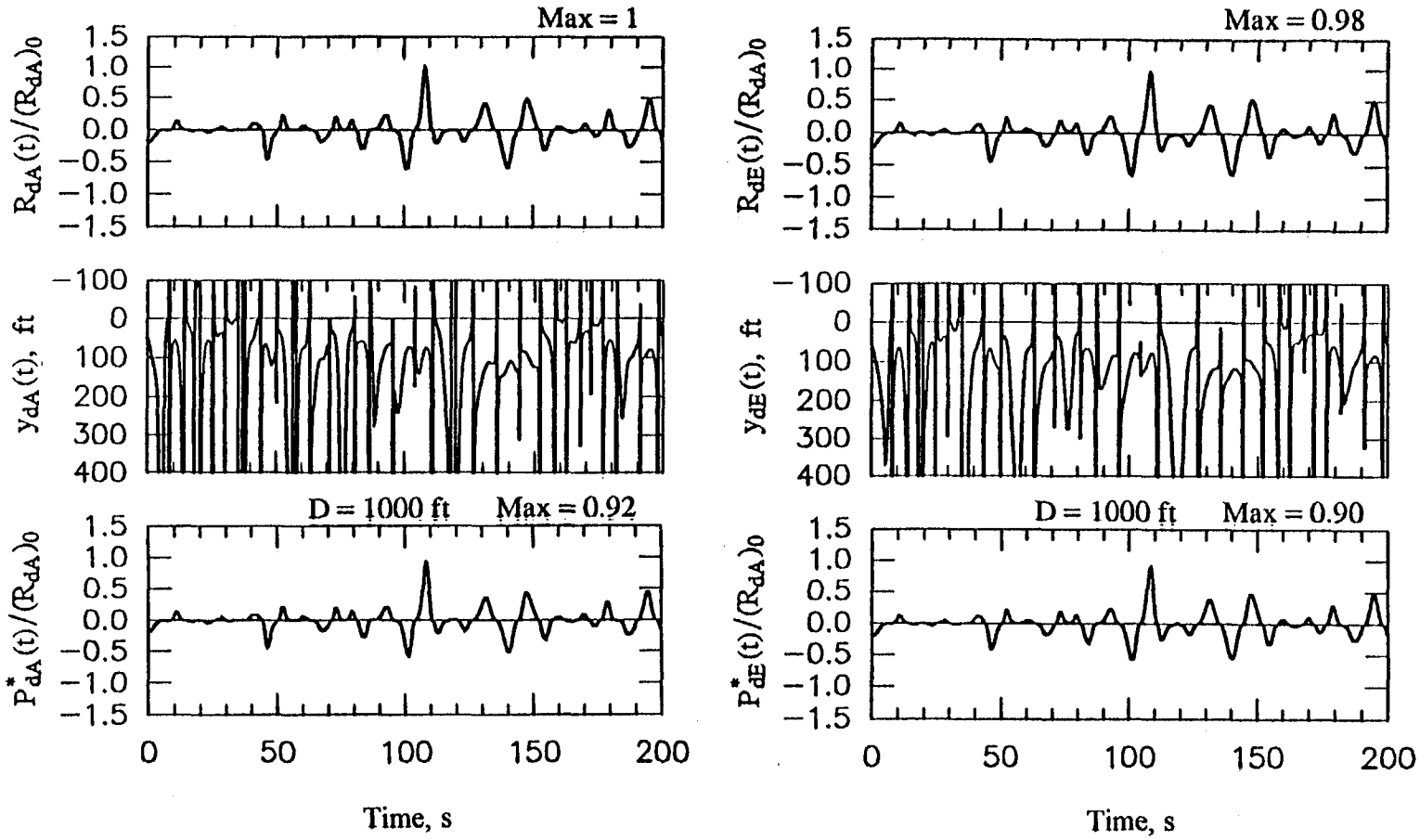

Fig. 4. Approximate and "Exact" Histories of $R_d(t)$, $y_d(t)$, and Corresponding Modal Forces.

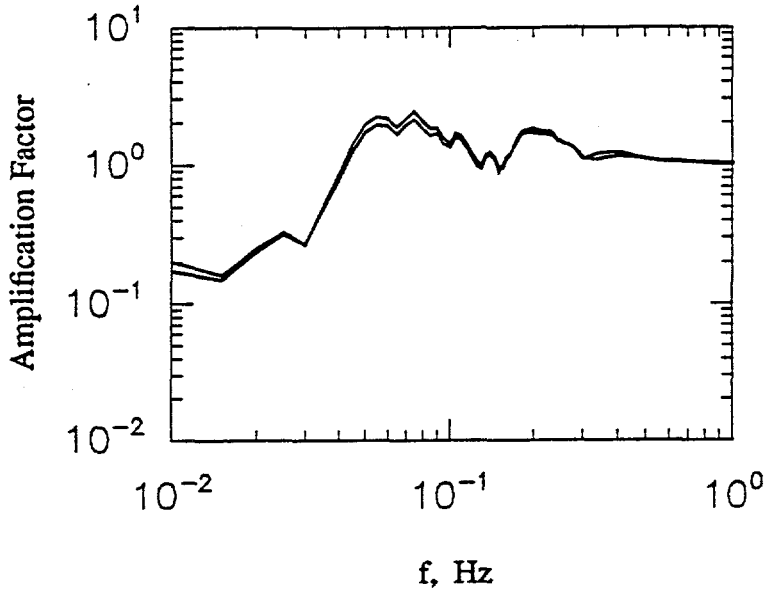

Fig. 5. Response Spectra for the Drag Modal Forces $P^{*}_{dA}(t)$ and $P^{*}_{dE}(t)$ Shown in Fig. 4; 5% Damping.

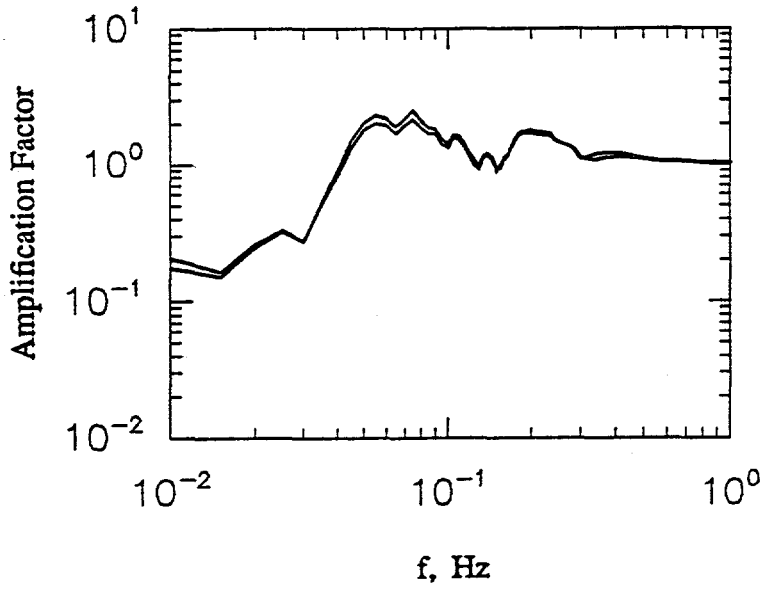

Fig. 6. Response Spectra for the Drag Forces $R_{dA}(t)$ and $R_{dE}(t)$ Shown in Fig. 4; 5% Damping.

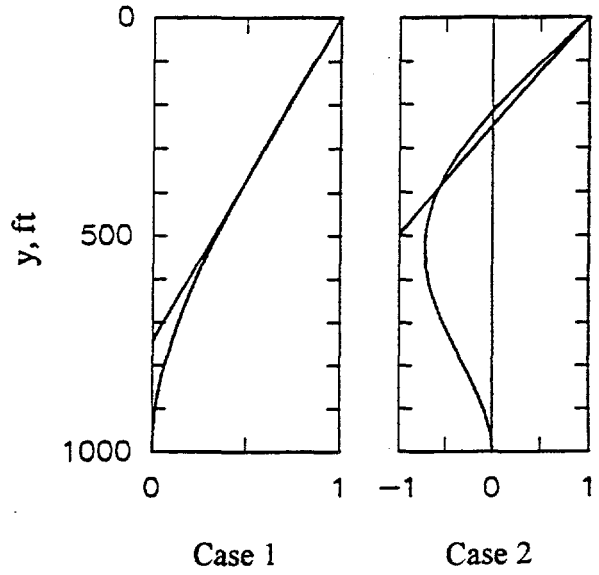

Fig. 7. Linear Approximations and Exact Variations for $B_m^*(y)/B_{m0}^*$ and $B_d^*(y)/B_{d0}^*$; $D = 1000$ ft.

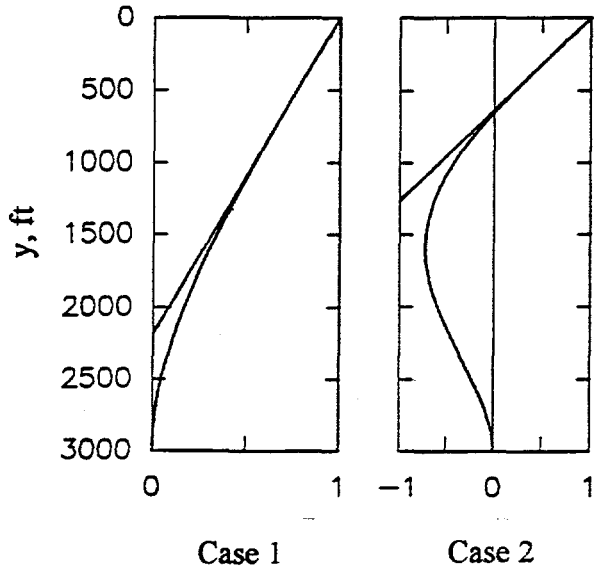

Fig. 8. Linear Approximations and Exact Variations for $B_m^*(y)/B_{m0}^*$ and $B_d^*(y)/B_{d0}^*$; $D = 3000$ ft.